Passive Synthetic Aperture Radar Imaging with Piecewise Constant Doppler Algorithm

Yijiang, Nan Xiaojing, Huang Y. Jay, Guo*

Abstract — **This paper presents a non-cooperative space-surface bistatic synthetic aperture radar (SS-BSAR) with a novel image reconstruction algorithm. Exploiting the continuous wave signal from the transmitters of opportunity, the new algorithm produces better imaging performance. Unlike the conventional passive SAR, the image reconstruction is achieved by correlation in time-domain without distinction between fast time and slow time. With the movement of the radar, the range curve can be linearized within multiple segments. In each segment, the Doppler frequency shift incurred in the reflected signal from a target can be assumed to be constant and thus the SAR image can be reconstructed recursively. The proposed piecewise constant Doppler (PCD) algorithm is validated by the simulation results.**

1 INTRODUCTION

As an alternative to active synthetic aperture radar (SAR), passive SAR imaging system has gained more and more attention due to its covert operation without intentional transmission [1, 2]. By using transmitters of opportunity as the source of scene illumination (e.g., GSM, analog TV, Digital Video Broadcasting-Terrestrial (DVB-T), DVB-S, DVB-S2, etc.), it can receive reflected and/or scattered signals off the Earths surface and/or other objects for various remote sensing and imaging applications. A typical passive SAR configuration is the bistatic one with stationary transmitter but moving receivers. For example, the DVB-S signal from a geosynchronous satellite can be used as the illuminator of opportunity and the radar receivers can be mounted on a moving platform such as an unmanned aerial vehicle (UAV). This system is known as the space-surface bistatic SAR (SS-BSAR) [1] .

Current passive SAR image processing algorithms are mostly based on a coherent summation of the received echo signals along the range curve, i.e., the change path of the propagation distance from the transmitter through the target to the receiver. To reduce the computational complexity, the more practical range Doppler algorithm (RDA) in passive SAR is commonly used [2]. However, RDA in passive SAR is still based on the stop-and-go approximation and thus leads to reduced image sampling rate in azimuth (i.e., slow time) and phase errors [3]. In addition, due to the continuously transmitted signal, RDA also introduces interference between samples in the range compressed image, thus further deteriorating the image quality. Moreover, for some passive SAR with cooperative transmitter, exact a *priori* information about the transmitter's parameters has to be estimated from the received reference signal.

In this paper, a non-cooperative SS-BSAR with novel image processing algorithm is proposed. The algorithm is based on time-domain correlation but significantly simplified by dividing the range curve into multiple segments with respective constant Doppler frequencies, and thus called piecewise constant Doppler (PCD) algorithm. Signal correlation between surveillance signal and reference signal in each segment can be recursively calculated with low complexity. The PCD algorithm does not make the stop-and-go approximation and eliminates the distinction between fast time and slow time, resulting in a high quality reconstructed image. In addition, due to the non-cooperative nature, no transmitted signal parameter is necessary other than the angle-of-arrival (AoA) of the incident beam, further reducing the signal processing complexity for signal parameter estimation and synchronization.

Detailed descriptions of the SS-BSAR configuration and the PCD algorithm are presented in this paper. Section II describes the SS-BSAR principle including the geometry and imaging process. The proposed PCD algorithm applied in passive SAR is derived in Section III and the numerical simulations are shown in Section IV. Finally, conclusions are drawn in Section V.

2 SS-BSAR PRINCIPLE

The considered passive SAR system is equipped with two receiving antennas to separate direct reference signal and surveillance echoes from the observed scene: the reference antenna looks toward the transmitter and the surveillance one looks toward the observed scene. The remaining direct power, which masks the weak surveillance signal, can be further removed using CLEAN techniques [4]. In this paper, we take the DVB-S as the source

*Global Big Data Technologies Centre, University of Technology Sydney, 81 Broadway, Ultimo NSW, Australia, e-mail: Yijiang.Nan@student.uts.edu.au, Xiaojing.Huang@uts.edu.au, Jay.Guo@uts.edu.au, tel.: +61 2 95142982.

of scene illumination. Since the observed scene is much farther from the satellite than the radar, the normalized incident angle of the DVB-S signal can be assumed as a constant, $\vec{I} = (a, b, c)$, where $a^2 + b^2 + c^2 = 1$, when the radar is traveling over the synthetic aperture.

2.1 Geometry and received signal

The system geometry is presented in Fig. 1. In the general 3-D Cartesian coordinates, the origin is set as the center of the observed scene (beam footprint), $P_c(0, 0, 0)$. The range and azimuth widths of the beam footprint are set to W and L respectively. The radar is mounted on the moving platform, which travels along the y-axis with the constant velocity v at a height h. The incident angle of the surveillance antenna is set to θ and the shortest slant range from the origin to the radar is set to R. Therefore, the radar's position can be expressed as $(-Rsin\theta, vt, h)$ and the slant range from an arbitrary point $P(x, y, 0)$ to the radar is

$$r_R(t, x, y) = \sqrt{(Rsin\theta + x)^2 + (y - vt)^2 + h^2} \quad (1)$$

where $t \in [y/v - T/2, y/v + T/2]$. T is the traveling time over the synthetic aperture, which is equal to L/v. The yellow plane illustrates the wavefront of the DVB-S signal which is received by the radar as the reference signal. The reference signal on the wavefront propagates toward the target $P(x, y, 0)$. It is reflected off the target and then received by the radar as the surveillance signal. Thus the difference of signal propagation path $r(t, x, y)$ between two antennas, illustrated as the red line, consists of the slant range $r_R(t, x, y)$ and the distance $r_T(t, x, y)$ from the imaging point P to this wavefront. $r_T(t, x, y)$ can be derived as

$$r_T(t, x, y) = |a(x + Rsin\theta) + b(y - vt) - ch| \quad (2)$$

where $t \in [y/v - T/2, y/v + T/2]$.

The relative motion between the radar and propgation direction of the DVB-S leads to a slight distortion in the received reference signal. As the radar moves along the y-axis, the wavefront across the radar will move forward or backward according to the AoA of the incident beam. Assuming that the transmitted DVB-S signal is defined as $s(t)$, the demodulated reference signal $s_{ref}(t)$ and surveillance signal $s_{sur}(t)$ can be expressed as

$$s_{ref}(t) = s(t + b \cdot vt)e^{j\frac{2\pi}{\lambda}b \cdot vt} \quad (3)$$

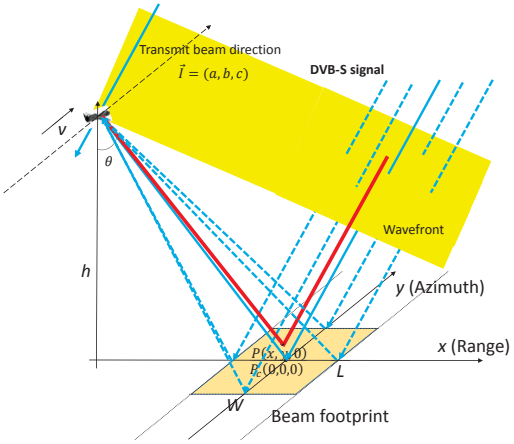

Figure 1: SS-BSAR geometry.

and

$$s_{sur}(t) = \int_{-\frac{W}{2}}^{\frac{W}{2}} \int_{vt-\frac{L}{2}}^{vt+\frac{L}{2}} \sigma(x, y) s_{ref}(t - \frac{r(t, x, y)}{c}) e^{-j\frac{2\pi}{\lambda}r(t,x,y)} dxdy \quad (4)$$

respectively, where $\sigma(x, y)$ is the radar cross section (RCS) of point (x, y), the center of beam footprint is $(0, vt)$, c is the light speed, and λ is the wavelength of the transmit beam.

2.2 Imaging process

Following the stop-and-go model, conventional passive SAR firstly divides the traveling time T into N_I blocks over the synthetic aperture and each block duration can be considered as a pulse repetition interval $PRI = T/N_I$ just like in conventional active SAR. Secondly, the range compression is done using the cross-correlation between the received reference and surveillance signals during each block time interval. After the range migration, the final focused passive SAR image is obtained by compensating each pixel's Doppler frequency shift according to the back-projection algorithm. The passive RDA converts the continuous wave signal into discrete samples with slow time sampling in azimuth and thus results in the poor imaging performance.

Actually, for each pixel of the observed scene, the imaging process is generally a cross-correlation over time period T between the surveillance signal and its location dependent reference signal. The most accurate and ideal imaging algorithm is thus to reconstruct an arbitrary pixel (x_i, y_i) according

to the equation

$$\int_{\frac{y_i}{v}-\frac{T}{2}}^{\frac{y_i}{v}+\frac{T}{2}} s_{sur}(t)s^*_{ref}(t-\frac{r(t,x_i,y_i)}{c})e^{j\frac{2\pi}{\lambda}r(t,x_i,y_i)}dt$$
$$=\int_{-\frac{W}{2}}^{\frac{W}{2}}\int_{y_i-\frac{L}{2}}^{y_i+\frac{L}{2}}\sigma(x,y)A_{x_i,y_i}(x,y)dxdy \tag{5}$$

where the corresponding ambiguity function is expressed as

$$A_{x_i,y_i}(x,y)=\int_{\frac{y_i}{v}-\frac{T}{2}}^{\frac{y_i}{v}+\frac{T}{2}} s_{ref}(t-\frac{r(t,x,y)}{c})$$
$$s^*_{ref}(t-\frac{r(t,x_i,y_i)}{c})e^{j\frac{2\pi}{\lambda}(r(t,x_i,y_i)-r(t,x,y))}dt \tag{6}$$

The beam footprint consists of a set of uniformly distributed pixels with spacings along x and y axises equal to the range and azimuth resolutions, δ_x and δ_y, respectively. From the knowledge of the position of pixels and the trajectory of the passive radar, the location dependent reference signal of any pixel can be reconstructed from the received reference signal directly. After performing correlation, the passive SAR finally reconstructs a two-dimensional image.

3 PIECEWISE CONSTANT DOPPLER ALGORITHM

Unfortunately, the abovementioned imaging algorithm can hardly work in practice. For a high resolution and wide-swath scene, the number of pixels is significant and leads to a great computational complexity. Aimed at reducing the complexity and the number of data storage, we propose a novel fast imaging algorithm in this section.

Assume that $r(t,x_i,y_i)$ satisfies the condition, $r(t,x_i,0)=r(t+\frac{y_i}{v},x_i,y_i)$. The difference in correlation outputs between two adjacent pixels in azimuth just involves a Doppler frequency shift and a little time delay, and thus the purpose of the PCD algorithm is to reconstruct the pixels recursively in azimuth. The Doppler frequency shift corresponds to the variation of range $r(t,x,y)$. The distance $r_T(t,x,y)$ varies linearly, resulting in a constant Doppler frequency shift, but the slant range $r_R(t,x,y)$ has non-linear variation. Therefore, we divide the entire correlation interval $[-T/2,T/2]$ into N_p segments and define the time instants at the junctions of these segments as $t_p=n_p\frac{T}{N_p}$ for $n_p=-\frac{N_p}{2},-\frac{N_p}{2}+1,...,\frac{N_p}{2}$. The segmentation, linearization and their relationship with the correlation are shown in Fig. 2. The recursive procedure in each segment can be further explained as follows.

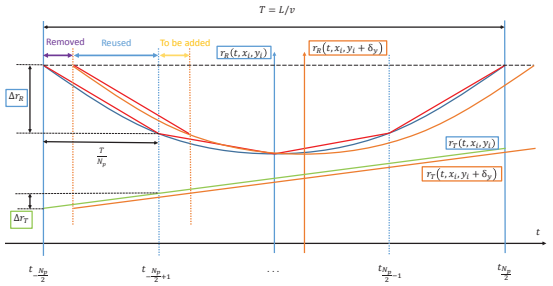

Figure 2: Over the synthetic aperture L, the bule line indicates the slant range r_R of the pixel (x_i,y_i), which can be piecewise linearized into the red line segments; Green line indicates the distance r_T; The orange lines indicate the r_R and r_T for the next azimuth pixel $(x_i,y_i+\delta_y)$.

Assume that the cross-correlation in an integration interval $[t_p,t_{p+1}]$ has been obtained for the pixel (x_i,y_i). To calculate the cross-correlation in the integration interval $[t_p+\delta_y/v,t_{p+1}+\delta_y/v]$ for the pixel $(x_i,y_i+\delta_y)$, we first remove the cross-correlation obtained in the interval $[t_p,t_p+\delta_y/v]$. It is easily seen in Fig. 2 that the correlation in the purple interval for the pixel (x_i,y_i) does not belong to the correlation for the pixel $(x_i,y_i+\delta_y)$. The second step is to compensate the Doppler frequency shift in the blue interval, which consists of two components: the first one is caused by the slant range difference,

$$r_{d_R}=r_R(t,x_i,y_i+\delta_y)-r_R(t,x_i,y_i)$$
$$=\frac{\delta_y N_p(r_R(t_p,x_i,0)-r_R(t_{p+1},x_i,0))}{Tv} \tag{7}$$

and the second one is caused by the difference of r_T,

$$r_{d_T}=r_T(t,x_i,y_i+\delta_y)-r_T(t,x_i,y_i)=\delta_y\cdot b. \tag{8}$$

As a result, Doppler frequency shift can be compensated by multiplying $e^{-j\frac{2\pi}{\lambda}(r_{d_R}-r_{d_T})}$. The final step is to add the new integration in the yellow interval which only belongs to the pixel $(x_i,y_i+\delta_y)$.

Instead of performing correlation operation for each pixel individually, the PCD algorithm updates the correlation result recursively and thus saves much data storage and reduces the computational complexity.

4 SIMULATION

We now consider a non-cooperative SS-BSAR with the following parameters: the antenna aperture is 1m, the radar velocity is 40m/s, the height of

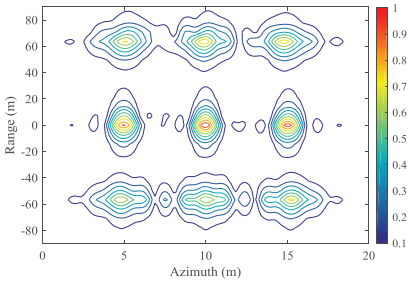

Figure 3: SAR image focused by RDA.

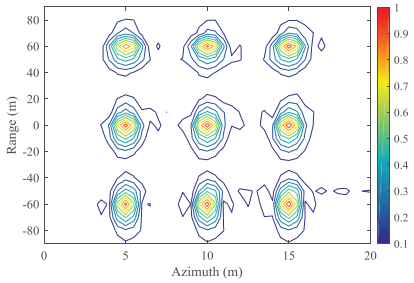

Figure 4: SAR image focused by PCD.

platform is 300m, the carrier frequency and bandwidth of DVB-S signal is 3GHz and 30MHz respectively, the normalized vector of AoA $\vec{I}$ is set to $(0.0099, -0.0995, 0.9950)$ and the incident angle of the radar θ is set to 45°.

Figs. 3 and 4 give the two 9-point final focused SAR images reconstructed by RDA and PCD algorithms respectively. In conventional passive SAR with RDA, the ranging compression is performed block by block along the synthetic aperture, resulting in the sampling in azimuth, known as the slow time. With continuous wave reference signal, the RDA will introduce interference in the range compressed image. The poor range compression will also have a negative impact on the further azimuth compression. Conversely, the PCD algorithm extends the integration interval to the synthetic aperture without distinguishing the slow and fast time, and thus the interference between segments can be neglected. It is evidently shown that except the central pixels, the imaging performance of PCD is superior to that of RDA in passive SAR.

Fig. 5 gives the correlation output in azimuth for an one-point SAR image. Assume that the N_I is set to 20. It is evidently seen that the azimuth ambiguity cannot be suppressed with the low azimuth sampling rate caused by the minimum antenna area constraint [3]. Conversely, the proposed SAR performs perfectly with the same number of segments $N_p = 20$, thus removing the limitation.

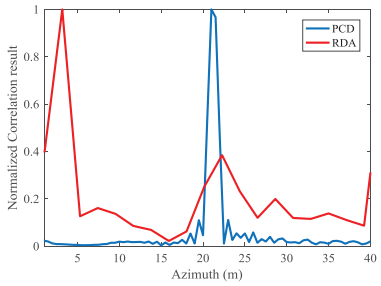

Figure 5: Azimuth imaging performance comparison between RDA and PCD

5 CONCLUSION

In this paper, we propose a non-cooperative SS-BSAR with PCD algorithm. The SAR image is reconstructed recursively along the flight path of the radar based on the constant Doppler frequency shift approximation in segmented range curve. The proposed SAR removes the the minimum antenna area constraint and extends the integration interval to the entire synthetic aperture, thus achieving a high resolution and wide-swath SAR image with good quality.

References

[1] M. Antoniou, M. Cherniakov, and C. Hu, "Space-surface bistatic sar image formation algorithms," *IEEE Transactions on Geoscience and Remote Sensing*, vol. 47, no. 6, pp. 1827–1843, June 2009.

[2] D. Gromek, K. Kulpa, and P. Samczyski, "Experimental results of passive sar imaging using dvb-t illuminators of opportunity," *IEEE Geoscience and Remote Sensing Letters*, vol. 13, no. 8, pp. 1124–1128, Aug 2016.

[3] A. Currie and M. A. Brown, "Wide-swath SAR," *IEE Proceedings F - Radar and Signal Processing*, vol. 139, no. 2, pp. 122–135, April 1992.

[4] K. Kulpa, P. Samczynski, M. Malanowski, L. Maslikowski, and V. Kubica, "The use of clean processing for passive sar image creation," in *2013 IEEE Radar Conference (RadarCon13)*, April 2013, pp. 1–6.